


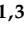




Article

# Beachrock Formation Mechanism Using Multiproxy Experimental Data from Natural and Artificial Beachrocks: Insights for a Potential Soft Engineering Method

Giannis Saitis <sup>1,\*</sup> , Anna Karkani <sup>1,\*</sup> , Eleni Koutsopoulou <sup>2</sup> , Konstantinos Tsanakas <sup>1,3</sup> , Satoru Kawasaki <sup>4</sup>  and Niki Evelpidou <sup>1</sup> 

<sup>1</sup> Faculty of Geology and Geoenvironment, National and Kapodistrian University of Athens, Panepistimiopolis, 15784 Athens, Greece; ktsanakas@hua.gr (K.T.); evelpidou@geol.uoa.gr (N.E.)

<sup>2</sup> Institute of Geology and Mineral Exploration, Acharnes, 54626 Athens, Greece; ekoutsop@upatras.gr

<sup>3</sup> Department of Geography, Harokopio University of Athens, 17671 Athens, Greece

<sup>4</sup> Faculty of Engineering, Hokkaido University, Kita 13, Nishi 8, Kita-ku, Sapporo 060-8628, Hokkaido, Japan; kawasaki@geo-er.eng.hokudai.ac.jp

\* Correspondence: saitij@geol.uoa.gr (G.S.); ekarkani@geol.uoa.gr (A.K.)

**Abstract:** Beachrocks are a window to the past environmental, geological, sedimentological and morphological conditions that were dominant in the coastal zone during their formation. Furthermore, beachrocks have the ability to reduce coastal erosion impact on sandy beaches. This study focuses on the beachrock formation mechanism through the comparison of cement characteristics, mineral chemistry and sedimentology of beachrock occurrences from two different geological and geographical localities: Diolkos, Corinth, Greece and Sumuide, Okinawa, Japan. In addition, in order to investigate a potential soft engineering method to protect coasts from erosion, artificial beachrock samples were created in vitro using sand samples and ureolytic bacteria from both areas under accelerating conditions. For Okinawa artificial beachrock experiments, the bacteria *Pararhodobacter* sp. was used, and for Diolkos, it was the bacteria *Micrococcus yunnainensis* sp. For the natural beachrocks, a multi-analytical approach was accomplished with the use of microscopic investigation, a scanning electron microscope, energy-dispersive X-ray spectroscopy, X-ray diffraction and X-ray fluorescence. Correlations were made between natural and artificial beachrocks. Results have shown that Diolkos beachrock was formed in the upper part of the intertidal zone, consisting of detrital material originating from the local bedrock, while Sumuide beachrock formed in the low intertidal–upper subtidal zone, consisting of coral sand and foraminifera fragments. For the artificial beachrocks, three samples were created using the microbial-induced carbonate precipitation (MICP) method, one from Diolkos (Corinth, Greece) and two from Sumuide (Okinawa, Japan). Diolkos artificial beachrock was better consolidated in comparison to Sumuide. Our investigation has shown that bacterial density was the key factor for the creation of the artificial beachrocks, while the samples' granulometry played a secondary role in the process. The laboratory artificial beachrocks show encouraging results for a new soft engineering method to encounter beach erosion while keeping an ecofriendly character by saving energy, material resources and gas emissions. Artificial beachrocks can share the same properties of a natural beachrock and can contribute positively to marine biodiversity as a natural rocky habitat.

**Keywords:** coastal erosion; MICP; cement; geomorphology; geochemistry; biocementation; Corinth; Greece; Okinawa; Japan



**Citation:** Saitis, G.; Karkani, A.; Koutsopoulou, E.; Tsanakas, K.; Kawasaki, S.; Evelpidou, N. Beachrock Formation Mechanism Using Multiproxy Experimental Data from Natural and Artificial Beachrocks: Insights for a Potential Soft Engineering Method. *J. Mar. Sci. Eng.* **2022**, *10*, 87. <https://doi.org/10.3390/jmse10010087>

Academic Editor: Patrick Hesp

Received: 5 December 2021

Accepted: 6 January 2022

Published: 10 January 2022

**Publisher's Note:** MDPI stays neutral with regard to jurisdictional claims in published maps and institutional affiliations.



**Copyright:** © 2022 by the authors. Licensee MDPI, Basel, Switzerland. This article is an open access article distributed under the terms and conditions of the Creative Commons Attribution (CC BY) license (<https://creativecommons.org/licenses/by/4.0/>).

## 1. Introduction

Sandy beaches represent almost 1/3 of the ice-free global coastline [1], hosting variable socioeconomic activities related to residency, recreation, tourism, industry, agriculture, aquaculture and fishing, conservation, military and even energy production plants [2,3].

Beach erosion poses a threat for all relevant stakeholders, and particularly for the tourism industry, according to the World Tourism Organization [4]. According to a recent study by Vousdoukas et al. [5], 13.6–15.2% of the world's sandy beaches might face beach regression by 2050, while these numbers may rise up to 35.7–49.5% by the end of 2100. The effects of coastal erosion will be accelerated by the effects of climate change, such as the intensity of storms and the global sea level rise, and by non-climatic factors, such as the reduction in the sediment supply associated with the anthropogenic modification of rivers and coastlines [6], whilst management will be complicated by concerns over hard engineering sea protection measures [7–10].

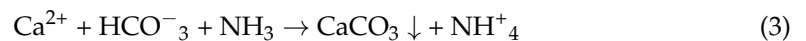
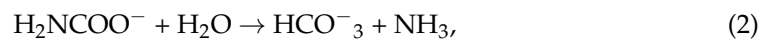
Traditionally, hard engineering structures, such as seawalls, groins, piers, etc., have been used to manage storms and tides for the protection of developments within the coastal zone [11]. However, these solutions are expensive, require long time periods and the engineering of large amounts of materials, and last but not least, as demonstrated in many cases, instead of preventing they often accelerate erosion at other nearby locations [6,7,11–13]. Furthermore, these techniques have a high impact on the natural coastal scenery, making it less appealing. Considering the above, alternative soft engineering techniques are needed to work in conjunction with natural coastal processes for a future with a sustainable coastal environment. The IPCC [14] has placed a greater emphasis on adaptation rather than impacts, reflecting a growing focus on integrated approaches by reducing risks that rely on flexible adaptation options and management [15]. A number of adaptation measures have been successfully implemented globally against coastal impacts and risks predominantly as a response to the current coastal risk or disasters experienced [16]. These need to be effective regardless of how environments change. Coastal management needs to shift to being more proactive than reactive, with a focus on planning then implementation, by emphasizing resilience, cost-effectiveness and working with nature. Furthermore, adaptive, sustainable planning should be undertaken in a wider socioeconomic development framework, considering societal needs, which often are more immediate than climate change.

Beachrocks are hard coastal deposits that consist of a wide variety of beach sediments, lithified at the shoreline through the precipitation of calcite and its magnesium polymorphs [17–22]. In beachrocks, the most common polymorph is high magnesium calcite (HMC > 5 mol %  $\text{MgCO}_3$ ) and aragonite (Ar) [17,23]. In the lower intertidal zone, beachrock cement consists of acicular aragonite forming isopachous fringes [24], while HMC cements form thin-bladed isopachous crusts or brown-colored micritic-sized crystal pelletal formations, sediment grain coatings and pores fillings [25–27]. On the other hand, cements of low-magnesium calcite with <5 mol %  $\text{MgCO}_3$  are indicative of the meteoricvadose zone. In terms of the beachrock formation mechanisms, four are dominant; three relate to the physicochemical conditions of cement precipitation [28], while the fourth concerns biochemical cement precipitation [29–31].

Beachrocks are most commonly found in the Mediterranean and Caribbean Seas, the tropical and subtropical Atlantic coasts, Brazil, Japan, Australia, as well as the atolls of the Pacific and Indian Oceans [17,32]. A particular characteristic of sandy beaches that host beachrocks is that they are less impacted from erosional processes and maintain their morphological and sedimentological characteristics [19,20,33,34]. Based on their protective role, recent studies have introduced an innovative, ecofriendly and sustainable technique to create artificial beachrocks in the laboratory by using microbial-induced carbonate precipitation (MICP) [35–38]. The MICP technique is a promising method where bacteria precipitate calcium carbonate and modify soil characteristics, resulting in soil consolidation and stabilization. Using MICP, it is possible to imitate the formation of natural beachrocks as countermeasure against erosion affecting sandy beaches by creating artificial rocks as a new soft engineering protection measure. Biocementation technology is a promising technology due to its suitability for field application [37]. The idea of creating artificial beachrocks in vulnerable beaches as an ecofriendly coastal sustainable application is to zero the  $\text{CO}_2$  emissions as this methodology does not involve concrete, energy-less consuming,

and this method uses natural energy sources by using local sand (in situ), thus achieving the reduction of building materials.

There are many variations of applying the MICP technique [39,40], and particularly, the urea hydrolysis method is the most protrusive for beachrocks creation. The MICP urea hydrolysis technique is described by reactions 1, 2 and 3 [41]:



In reaction 1, urea is hydrolyzed by urease (this reaction is called ureolysis) to produce carbamate and ammonium ions. In reaction 2, we observe the carbamate ion being hydrolyzed and producing an ammonia molecule and bicarbonate. Finally, in reaction 3, the diluted calcium ions are reacting with bicarbonate and ammonia to produce pre-calcium carbonate, which precipitates and forms the cement.

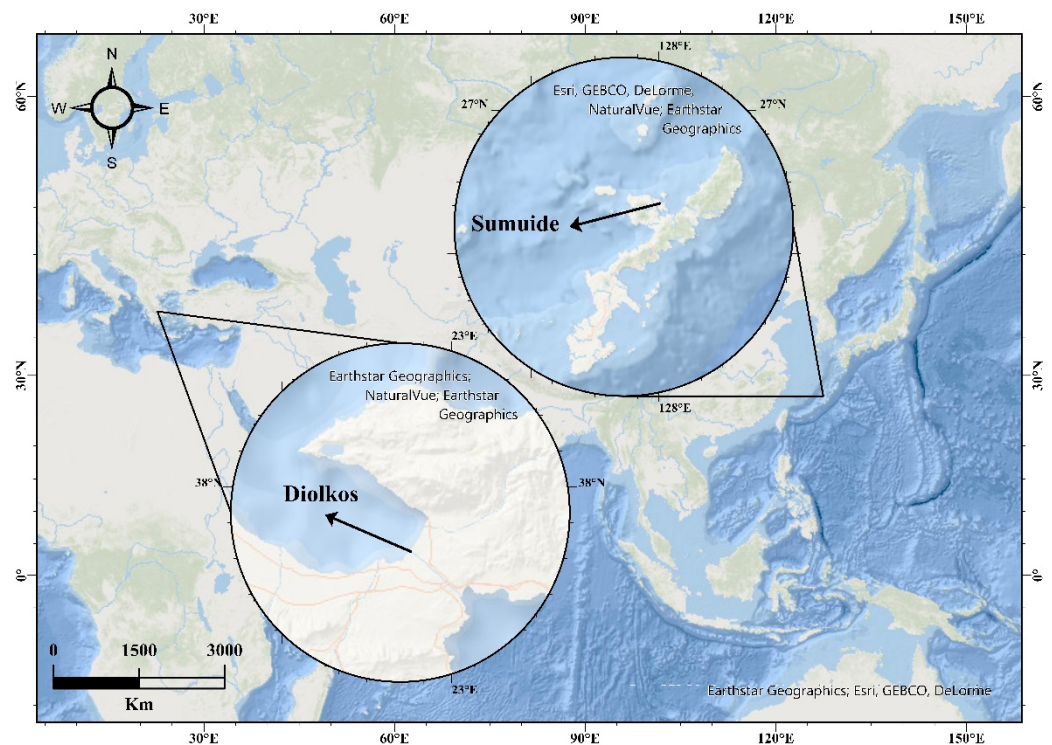
In this context, this study aims to provide an insight into a new soft engineering solution for protecting the vulnerable coastal zone from erosion. In order to achieve the aforementioned, we studied the beachrock cementation process by comparing the characteristics of natural beachrocks and the in vitro artificial beachrocks in terms of their mineralogical and geochemical properties. For the purposes of this study, two case studies are examined from different geological and geographical settings: Corinth, Greece and Okinawa Island, Japan. For the creation of artificial beachrocks, samples of local sand and bacteria of both study areas were used for three MICP experiments. A multi-analytical approach was used for the study of beachrocks, including petrographic microscopy, a scanning electron microscope (SEM) equipped with energy dispersive X-ray microanalysis (EDX) and X-ray diffraction (XRD).

## 2. Geographical and Geological Setting

### 2.1. Diolkos, Corinth, Greece

The Diolkos site is located at the Gulf of Corinth (Figure 1), a prominent tectonic and geomorphological structure, in the central part of Greece, segregating the Peloponnese to the south and Central Greece to the north. Most of Corinth's geological basement consists of Triassic to Jurassic grey limestones of the Sub-Pelagonian zone. The Corinth canal is composed of a series of faulted Pliocene–Pleistocene marls, limestones, sandstones and conglomerates [42].

The Diolkos site lies on the south coasts of the Isthmus canal. It is characterized by an extend beachrock outcrop, which is divided by the Corinth canal into the north and south. The beachrocks are located approximately 1 m above sea level (a.s.l.) [43]. The small beaches hosting the beachrocks are characterized by medium-sized grains to gravels. The studied beach has a North–South orientation with a 10° inclination. At the southern beachrock outcrop, the remnants of Diolkos are visible. Diolkos was an ancient slipway used for transporting ships from the Corinth Gulf to Saronic Gulf and vice versa. This road was used for transporting ships with the help of a wheeled vehicle, where the ships were moored, once exempt from their cargo, in the docks of Cenchreae or Lechaion.



**Figure 1.** Location of study areas. In the west is Diolkos, Corinth, Greece, while in the east is Sumuide, Okinawa Island, Japan.

## 2.2. Sumuide, Okinawa, Japan

Okinawa is the largest of the Okinawa Islands and the Ryukyu Islands of Japan. The island covers an area of 1206 m<sup>2</sup> and it is located 640 km south from the main island of Japan. The Ryukyu Islands extend from Kyushu in the north, to Taiwan in the south and exceed 1200 km in length.

Covering an area of about 150,000 km<sup>2</sup>, the Okinawa Trough is an active back-arc rift-basin between the East China Sea (ECS) Sheff Basin/Taiwan-Sinzi belt and the Ryukyu arc, since at least the late Miocene era [44], and it is the youngest back-arc rift-belt in the East China Sea. Although the Okinawa Trough mainly consists of igneous/volcanic rocks and Miocene sedimentary rocks, its basement comprises Paleogene and Mesozoic sedimentary sequences. The Ryukyu group is composed of a large number of reef complex deposits, with proximal water coral limestone and distal rhodolith and detrital limestones [45].

Beachrock outcrops are regularly distributed around Okinawa Island. Many studies have been published in recent years about beachrocks in Okinawa and their formation [20,31,46,47]. Evelpidou et al. [20] studied seven beachrock sites in the central western, south, central eastern and north parts of Okinawa Island. All beachrock occurrences extended no more than 1 m a.s.l. to a few centimeters below sea level (b.s.l.). In this study, we focus on the beachrock outcrop at Sumuide site, which is located in the central northern part of Okinawa Island (Figure 1).

## 3. Materials and Methods

### 3.1. Fieldwork

Field investigation included detailed spatial mapping of the beachrock outcrops in both studied sites. Transects were carried out in order to (i) measure the width and elevation/depth of beachrock slabs (with respect to mean sea-level) and (ii) sample the top beds of the front (seaward) and the end (landward) of each beachrock slab [19,20,48–50]. At the Sumuide site (Okinawa, Japan), GPS measurements were performed with an accuracy of  $\pm 5$  cm and the elevation/depth of beachrocks were measured using a 3 m metallic bar with

20 cm division. At the Diolkos site (Corinth, Greece), both coordinates and elevation/depth were measured using a DGPS-GNSS Spectra SP60 system, with an accuracy of  $\pm 3$  cm.

Beachrock samples were collected from both sites; 6 samples were obtained from Diolkos, due to the irregular shape of the outcrop, and 2 samples were from Sumuide. In addition, samples of sand were collected from the overlying sediment of beachrocks from both studied sites to be used for solidification testing to create the in vitro beachrocks. The samples were stored in sterile tubes to avoid any contamination.

### 3.2. Artificial Beachrocks

#### 3.2.1. Screening and Cultivation of Bacteria

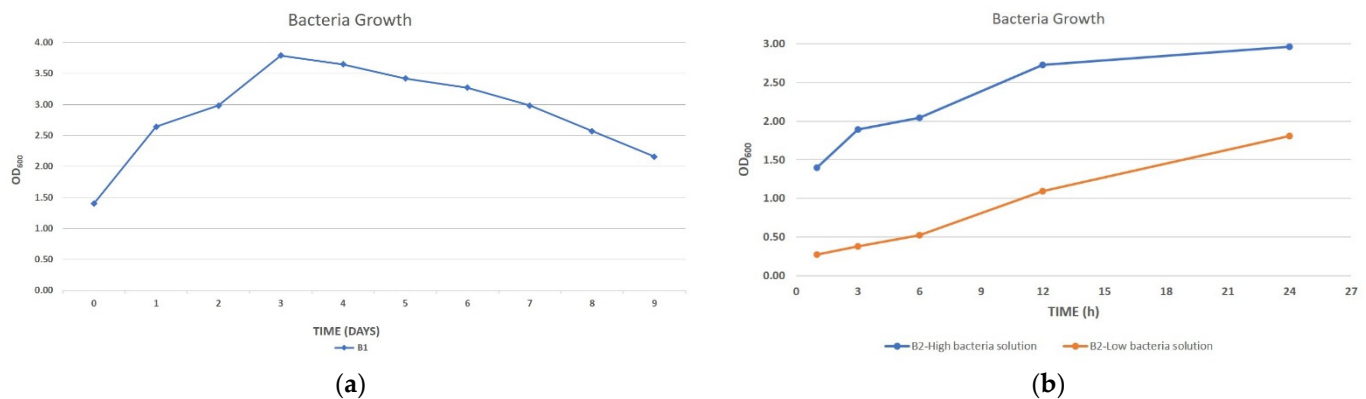
In our study, we used the bacteria *Micrococcus yunnanensis* sp. (Bacteria B1) isolated from the beach sand of the Diolkos site [51] and the bacteria *Pararhodobacter* sp. (Bacteria B2) from the Sumuide site [52]. Both bacteria species were identified by 16S rRNA gene analysis and were used for the calcium carbonate precipitation. A ZoBell2216E medium (5.0 gr/L polypeptone, 1.0 gr/L yeast extract, and 0.1 gr/L  $\text{FePO}_4$  was prepared in artificial seawater (Table 1), adjusted to pH 7.6–7.8) was used as the culture medium for cultivating the bacteria. The isolated bacteria were pre-cultured in 5 mL medium at 30 °C with shaking at 160 rpm for 24 h. One milliliter of the pre-culture was inoculated into 100 mL of ZoBell2216E medium incubated at 30 °C while shaking it at 160 rpm. During cultivation, bacteria cell concentration was determined by measuring the absorbance (Optical Density, OD) of the suspension using a UV-vis spectrophotometer (V-730, JASCO Corporation, Tokyo, Japan) at a 600 nm wavelength ( $\text{OD}_{600}$ ). During cultivation, we used a 0.5 M ZoBell2216E medium for the bacteria *Micrococcus yunnanensis* sp. and *Pararhodobacter* sp. and a 0.3 M ZoBell2216E medium for only *Pararhodobacter* sp.

**Table 1.** Composition of artificial sea water (solvent: distilled water).

Chemical Composers	[gr/L]
$\text{MgCl}_2 \cdot 6\text{H}_2\text{O}$	222.23
$\text{CaCl}_2 \cdot 2\text{H}_2\text{O}$	30.70
$\text{SrCl}_2 \cdot 6\text{H}_2\text{O}$	0.85
KCl	13.89
$\text{NaHCO}_3$	4.02
KBr	2.01
$\text{H}_3\text{BO}_3$	0.54
NaF	0.06
NaCl	490.68
$\text{Na}_2\text{SO}_4$	81.88

Additionally, we applied a urease activity test using Cresol Red solution. By measuring the bacteria concentration  $\text{OD}_{600}$ , we obtained for the bacteria *Micrococcus yunnanensis* sp. the growth curve of the microbial strain. Two growth curves of bacteria *Pararhodobacter* sp. were obtained, one for the 0.5 M medium solution, which led to a high-concentration bacteria solution, and one for the 0.3 M medium solution, which led to a low-concentration solution (Figure 2).





**Figure 2.** Bacterial growth curves using Optical Density value 600 nm (OD<sub>600</sub>). (a) For experiment 1, the bacteria B1 was monitored for 9 days. (b) For experiments 2 and 3, the bacteria B2 was monitored for 24 h.

### 3.2.2. Experimental Conditions

The MICP artificial beachrock experiment was implemented by using three different solidification scenarios. From hereinafter, the three scenarios will be numbered as experiments 1, 2 and 3.

Experiment 1 involved beach sand samples from Diolkos area and the bacteria *Micrococcus yunnanensis* sp. (B1). For the experiment setting, 1 kg of beach sand was sieved using six mesh sizes to separate gravel (>2 mm), sand (1 mm, 500 µm, 250 µm, 125 µm, 63 µm) and silt/clay particles (<63 µm). Samples were oven-dried at 80 °C. For the artificial beachrock experiment, the grain size composition used corresponds to the granulometry of Diolkos beach, i.e., 26.5% gravels, 72% sand and 0.5% silt/clays. Furthermore, the bacteria density and the CaCO<sub>3</sub> content were maintained as stable during the experiment, operated at 25 °C.

Experiments 2 and 3 concerned sand samples from the Sumuide site and the bacteria *Pararhodobacter* sp. (B2). The sand samples consisted of calcareous material, which was sieved using two mesh sizes to separate gravel (>2 mm) and coarse and medium sand (1 mm). The sand used for both experiments had a grain size of 1 mm. Additionally, for both experiments (2, 3) the CaCO<sub>3</sub> content and temperature (30 °C) were kept stable. However, the two experiments differed in the concentration of bacteria solution; for experiment 2 a high-concentration solution was used, while for experiment 3, we used a low one.

### 3.2.3. Syringe Solidification Test

Sterilized sand samples from Diolkos and Sumuide beaches were prepared in syringes of 50 mL and 35 mL volume, respectively. In the syringes, 85.5 gr of Diolkos sand (experiment 1) and 40 gr of coral sands (experiment 2 and 3) were used, along with three bacteria reagents.

During the solidification experiments, in order to prepare the bacteria B1 reagent for experiment 1 and the two bacteria reagents of high and low bacteria B2 concentration for experiment 2 and 3, respectively, the density of bacteria and their growth was determined in the solutions using the Optical Density value of 600 nm by UV-VIS spectrophotometer (UV-2500PC SHIMADZU). The number of bacteria in the solution of experiment 1 were measured for 9 days and in the experiments 2 and 3 for 24 h.

Following the experiment, ZoBell2216E culture medium solution was prepared using artificial seawater as solvent. The culture medium and artificial seawater solution was inoculated with 0.1 gr per 100 mL solution of bacteria B1 for experiment 1, and with bacteria B2 for experiments 2 and 3. Then, all were incubated at 30 °C while shaking them at 80 rpm for 3 days.

Meanwhile, 80 gr of Diolkos sand for experiment 1 and 40 gr of coral sand for experiments 2 and 3 were dried at 100 °C for 2 days and placed in a 50 mL and 35 mL syringe,

respectively. Subsequently, for experiment 1, we prepared 25 mL of B1 bacterial culture along with 30 mL of 0.5 M solidification solution (Table 2). For experiments 2 and 3, 16 mL of B2 bacterial cultures (high and low concentration) along with 20 mL of solidification solution were sequentially injected into the syringe and drained out, while having the sand saturated with 2 mL of solution above the surface of the cement.

**Table 2.** Chemical composition of a 0.5 M solidification solution used during the artificial beachrock experiment.

Chemical Components	Amounts
Artificial seawater	100 mL
Nutrient Broth	0.3 gr
NH <sub>4</sub> Cl	1 gr
(NH <sub>2</sub> ) <sub>2</sub> CO	3 gr
NaHCO <sub>3</sub>	0.212 gr
CaCl <sub>2</sub>	5.55 gr

After curing the sand samples of experiments 1, 2 and 3 with their corresponding bacterial solutions, the consolidation solution was injected from the top of the syringe and drained out from the bottom at fixed intervals of 24 h for 14 days. The Ca<sup>2+</sup> concentration and pH of the drainage outlet were also measured to determine temporal variations of these parameters in the samples. pH and Ca<sup>2+</sup> are indicators of the urease hydrolysis taking place in the samples. For Ca<sup>2+</sup> measurement, a LAQUA twin (HORIBA) was used, while for the pH, we used an electronic portable pH meter. For experiment 1, the Ca<sup>2+</sup> and pH measurements were taken daily. For experiments 2 and 3, measurements were taken on days 3, 6, 9, 12, and 14 of the experiment.

It should be noted that in the middle of the experiment (day 7), we reinjected the bacteria solution in order to rejuvenate the bacteria in the syringe test.

### 3.2.4. Solidification Determination

After 14 days of the solidification experiments, the samples were extracted from the syringes. A needle penetration device (SH-70, Maruto Testing Machine Company, Tokyo, Japan) was used to calculate the penetration inclination (Np) and estimate the unconfined compressive strength (Newton/mm = Pressure N/m<sup>2</sup>, needle's head area is inconsiderable) [36–38,52]. The UCS was estimated by needle penetration test.

All consolidated samples were approximately 7 cm in length. The needle penetration test was applied on 3 parts of the sample: upper, middle, and bottom, with a mean step of 2 cm.

### 3.3. Mineralogy and Geochemical Analysis

Mineralogical and geochemical analyses were conducted at the laboratory of the Department of Mineralogy and Petrography, Institute of Geology and Mineral Exploration, Athens, Greece and the laboratory of Economic Geology and Geochemistry at the Faculty of Geology and Geoenvironment of the National and Kapodistrian University of Athens.

The natural beachrock samples from Diolkos and Sumuide and their corresponding artificial samples were analyzed for the determination of their mineralogical composition and textural characteristics with a LEICA-DMLP (Leica Microsystems GmbH, Wetzlar, Germany) petrographic microscope equipped with a digital camera. The identification of minerals by their color is based on the method of Michel-Lévy Interference Color Chart.

The bulk mineralogy of the natural beachrock samples was analyzed using the X-ray diffraction (XRD) method. In the case of natural Diolkos samples, a Panalytical X'pert-Pro X-ray diffractometer was used, equipped with a Cu X-ray tube (K $\alpha$  of Cu,  $\lambda$  = 1.5405 Å), a graphite monochromator, an applied voltage of 30 kV and a 40 mA current. The random powder mounts of samples, prepared by back loading, were scanned from 2° to 70° 2 $\theta$ . Powder diffraction data were collected at room temperature. Data were evaluated with

the X'Pert High-Score (Version 2004) (PANalytical B.V., Almelo, The Netherlands). Further XRD analyses were also conducted on the natural and artificial beachrock samples from Sumuide. X-ray diffraction measurements were carried out on a Bruker Model 5005 X-ray diffractometer in combination with the DIFFRAC plus software package. The diffractometer was operated using Cu K $\alpha$  radiation at 40 kV and 40 mA with a graphite monochromator. In Sumuide cases, the XRD output files were evaluated for mineralogical identifications using the EVA<sup>®</sup> software provided by Bruker (DIFFRACplus software EVA, Bruker AXS GmbH) (Bruker Corporation (2006), DIFFRACplus EVA v12.0.) and managed with the PDF-2 database (International Centre for Diffraction Data, Newtown Square, PA, USA).

The chemical composition of Diolkos natural beachrock minerals was examined under scanning electron microscopy (SEM) using a JEOL JSM-5600 equipped with an Oxford Link Energy Dispersive Spectrometer (EDS) (Oxford Instruments). Microanalyses were performed on epoxy resin-impregnated polished and carbon-coated thin sections. The measured concentrations were automatically corrected for atomic number, absorption in the sample, fluorescence and dead time (the ZAF correction) using the INCA software. The chemical composition of the minerals was determined using natural minerals and synthetic oxide standards, and 20 kV accelerating voltage with 1.5 nA beam current and 50 s dead time. Studies were carried out using backscattered images to ensure the maximum output of information. The contrast in the image produced is determined by the atomic number of the elements in the sample. Therefore, the image shows the distribution of different chemical phases in the sample and produces valuable information on the morphology of the studied samples. The chemical composition of Sumuide natural and artificial beachrock samples were studied at Hokkaido University laboratories under SEM-EDX using a SHIMADZU SUPERS CAN SSX-550 and using the same aforementioned analytical methodology under 15 kV accelerating voltage.

The concentrations of major and trace elements in bulk samples of Diolkos natural beachrocks were defined using energy dispersive X-ray fluorescence spectroscopy (EDS-XRF, S4 Ranger, Bruker). Loss on ignition (LOI) was determined from the weight loss after heating 1 gr of sample (previously dried at 105 °C) for 1 h at 1000 °C. XRF analysis was not applied on Sumuide natural beachrock samples due to the main calcite composition and the difficulty to distinguish the cement composition from the calcareous beach grains.

## 4. Results

### 4.1. Results on the Natural Beachrocks

#### 4.1.1. Beachrock Distribution

At the Diolkos site, the beachrock has a mean dip of 12.5° seawards. Its maximum width is about 30 m. The outcrop's maximum height above the mean sea level is 1.10 m. The outcrop has no evidence of erosional rims (channels) perpendicular to the shoreline on its surface. The channel of Corinth is protected by a sea wall where the examined beachrock is located. In addition, manmade structures have been noticed to be incorporated into the beachrock outcrops.

Sumuide beach is oriented West–East and the examined beachrock extends parallel to the coast with an average length of 127 m and a seaward dip of 3.5°. Its mean width is 12 m with a maximum height above the mean sea level of about 70 cm. Quarrying marks are evident on the outcrop, while there are also erosional features from the wave energy.

#### 4.1.2. Beachrock Lithology

Diolkos beachrock samples are characterized by a coherent pattern with sub-rounded and well-to-medium sorted grains and the general absence of bioclasts (<3%). The lithoclasts mainly consist of quartz, calcite, dolomite, plagioclase, K-feldspar.

For Sumuide beachrock, the seaward sample, Sum1, has poorly rounded and medium sorted lithoclasts, while its lithology consists mostly of calcite, quartz, dolomite and mica with a high presence of bioclasts ( $\geq 60\%$ ). On the other hand, the landward sample, Sum2,



has medium rounded and sorted lithoclasts and grains, which consist mostly of calcite and aragonite with a high presence of bioclasts ( $\geq 50\%$ ) (Table 3).

**Table 3.** Physico-chemical characteristics of natural beachrocks from Diolkos and Sumuide areas and their corresponding artificial beachrock. Their micromorphology is based on SEM and microscopic examination. Main mineral components were also confirmed by XRD analysis. Microcrystalline HMC was observed as main cement component.

Samples	Elevation (m) (RSL)	Component Materials	Main Mineral Compound	Cement Composition and Microstratigraphy	Cementation Precipitation Mechanism
Natural beachrocks					
Diolkos 1 (Kodi1)	+0.32	Sub-rounded, medium to well sorted lithoclasts grains. No bioclasts	Quartz, Mg-Calcite, Calcite, Dolomite, Albite, Serpentine, Illite and Chlorite	Thin isopachous micritic HMC. Brown bio-micritic cement. Matrix infilling	Shallow intertidal zone, marine vadose sone with marine and freshwater mixture. Mainly physicochemical precipitation, low bioactivity.
Diolkos 2 (Kodi2)	+0.26	Sub-rounded, medium to well sorted lithoclasts grains. No bioclasts	Quartz, Mg-Calcite, Calcite, Dolomite, Albite, Serpentine, Illite and Chlorite	Thin isopachous micritic HMC and brown bio-micritic cement. Matrix infilling	
Diolkos 3 (Kodi3)	+0.53	Sub-rounded, bad sorted lithoclasts grains. No bioclasts	Quartz, Mg-Calcite, Calcite, Dolomite, Albite, Serpentine, Orthoclase, Illite and Chlorite	Thin isopachous micritic HMC. Pellet concentrations. Partially matrix infilling	
Diolkos 4 (Kodi4)	+0.22	Sub-rounded, bad sorted lithoclasts grains. No bioclasts	Quartz, Mg-Calcite, Calcite, Dolomite, Albite, Serpentine, Orthoclase, Illite and Chlorite	Thin isopachous micritic HMC and brown bio-micritic cement. No matrix	
Diolkos 5 (Kodi5)	−0.20	Sub-rounded to well rounded, well sorted lithoclasts grains. No bioclasts.	Quartz, Mg-Calcite, Calcite, Dolomite, Albite, Orthoclase, Illite and Chlorite	Thick isopachous micritic HMC and brown bio-micritic cement. Meniscus forms. No matrix.	
Diolkos 6 (Kodi6)	+0.05	Sub-rounded, bad sorted lithoclasts grains. Algae parts.	Quartz, Mg-Calcite, Calcite, Dolomite, Albite, Orthoclase, Illite	Thick isopachous micritic HMC and brown bio-micritic cement. Cement fills the pores.	
Sumuide 1 (Sum1) (Evelpidou et al., 2019)	+0.95	Poorly rounded, medium sorted lithoclasts grains. High contribution of bioclasts.	Calcite, Quartz, Mg-Calcite, Dolomite, Mica	Thick HMC in microcrystalline and sparitic form. Matrix infilling	Intertidal zone, physicochemical precipitation, medium microbial activity.
Sumuide 2 (Sum2)	+0.71	Medium rounded and sorted lithoclasts, grains. High contribution of bioclasts.	Mg-Calcite, Aragonite	Thick calcite and HMC in microcrystalline and sparitic form with presence of Aragonite crystals. Matrix infilling.	Intertidal zone, physicochemical precipitation, medium microbial activity.

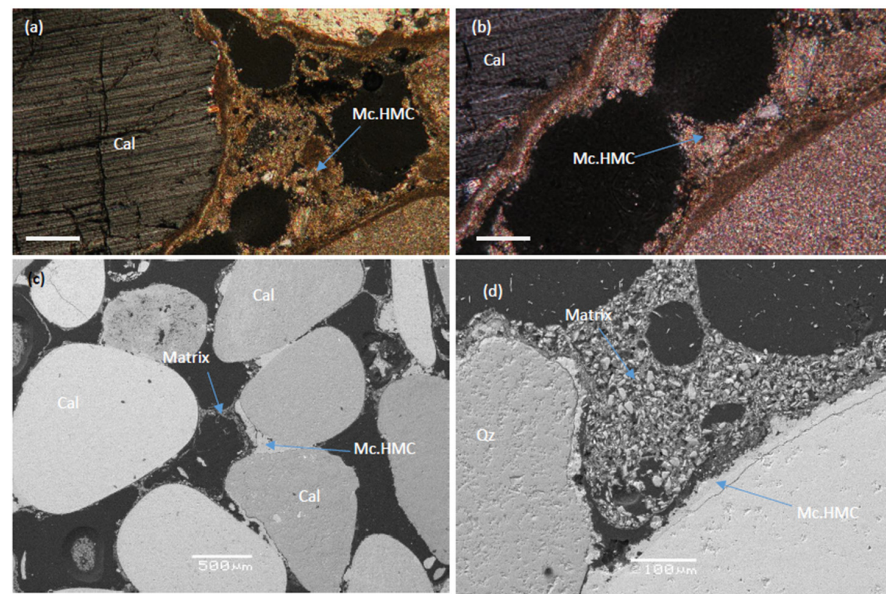
Table 3. Cont.

Samples	Elevation (m) (RSL)	Component Materials	Main Mineral Compound	Cement Composition and Microstratigraphy	Cementation Precipitation Mechanism
Artificial beachrocks					
ArDi1	-	Sub-rounded, bad sorted lithoclasts grains. Small presence of bioclasts.	Calcite	Mostly micritic and spirititic calcite cement. Irregular thickness 10–100 $\mu\text{m}$ . A fan form grain coating, meniscus forms and pore filling.	-
ArSum1	-	Rounded, bad sorted grains. High contribution of bioclasts.	Aragonite- Calcite	Well-developed aragonite crystals 10–20 $\mu\text{m}$ . Micritic calcite as pore filling.	-
ArSum2	-	Rounded, bad sorted grains. High contribution of bioclasts.	Aragonite	Well-developed aragonite crystals.	-

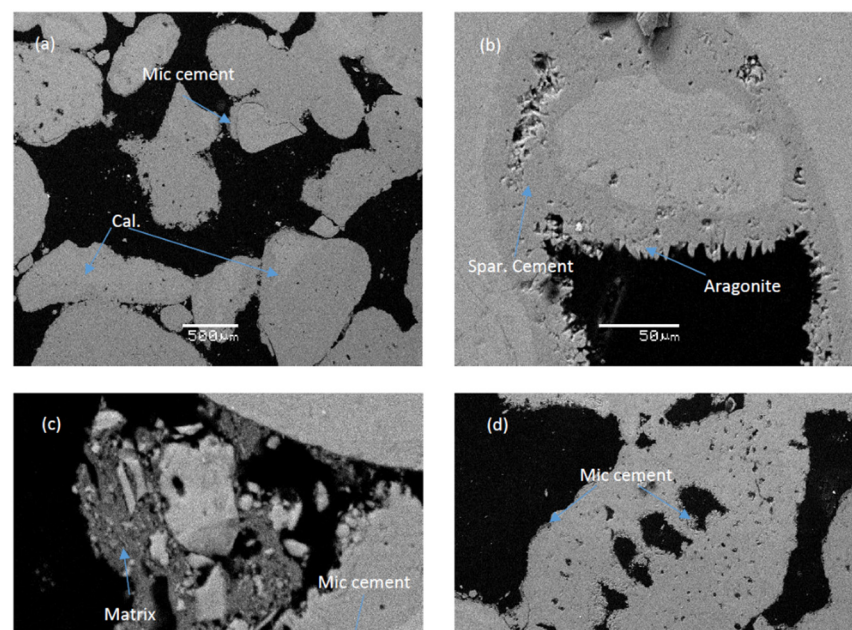
#### 4.1.3. Cement Composition

The examination of the beachrock cements from Diolkos showed that the micritic HMC  $[(\text{Ca},\text{Mg})\text{CO}_3]$  cement was the most dominant in all samples, identified using backscattered electron images (BSE) and EDS analyses. In the samples Kodi1, Kodi2, Kodi3 and Kodi4, the cement forms a thin isopachous coating around the sediment grains. On the other hand, the samples Kodi5 and Kodi6 are characterized by a thick isopachous coating of micritic HMC cement. Following the coating cementation, a brown micritic cement forming an outer cover was identified in almost all samples, with the exception of Kodi3. A pore filling matrix cement was observed, consisting of very fine sedimentary particles (5–20  $\mu\text{m}$ ) and micritic HMC in the samples Kodi1, Kodi2 and Kodi3. In the samples Kodi3 and Kodi5, a pellet cement formation was identified, while in the latter meniscus, cement formation was also noted (Table 3) (Figure 3).

Both samples from Sumuide (Sum1 and Sum2) were characterized by the same cement type of HMC, and by isopachous micritic and sparitic crystals (rhomboidal crystals) along with needle-like crystals of aragonite. Furthermore, matrix cement was also identified as pore filling. The cement texture can be generally characterized as micritic with the presence of interclasts, while also forming meniscus and peloidal concentrations (Figure 4).



**Figure 3.** Polarized microscopy image: (a) sample Kodi2, 10× magnification, scale 20  $\mu\text{m}$ . Micritic HMC cement is coating calcite grains; (b) sample Kodi2, 20× magnification, scale 10  $\mu\text{m}$ . Micritic HMC cement is coating calcite grains. SEM images: (c) sample Kodi 6, micritic cement is coating calcite grains, the matrix consists of very fine sedimentary particles; (d) sample Kodi6, micritic cement is coating calcite and quartz grains, while the matrix consists of very fine sedimentary particles and micritic HMC cement.



**Figure 4.** SEM images of sample Sum1: (a) well-crystalized calcite and aragonite needles are coating calcite grains and microfossils that are consolidated; (b) sparitic cement and aragonite are precipitated inside a microfossil; (c) micritic cement with the matrix consisting of very fine sedimentary particles; (d) micritic cement that is coating a microfossil and is precipitated inside its vents.

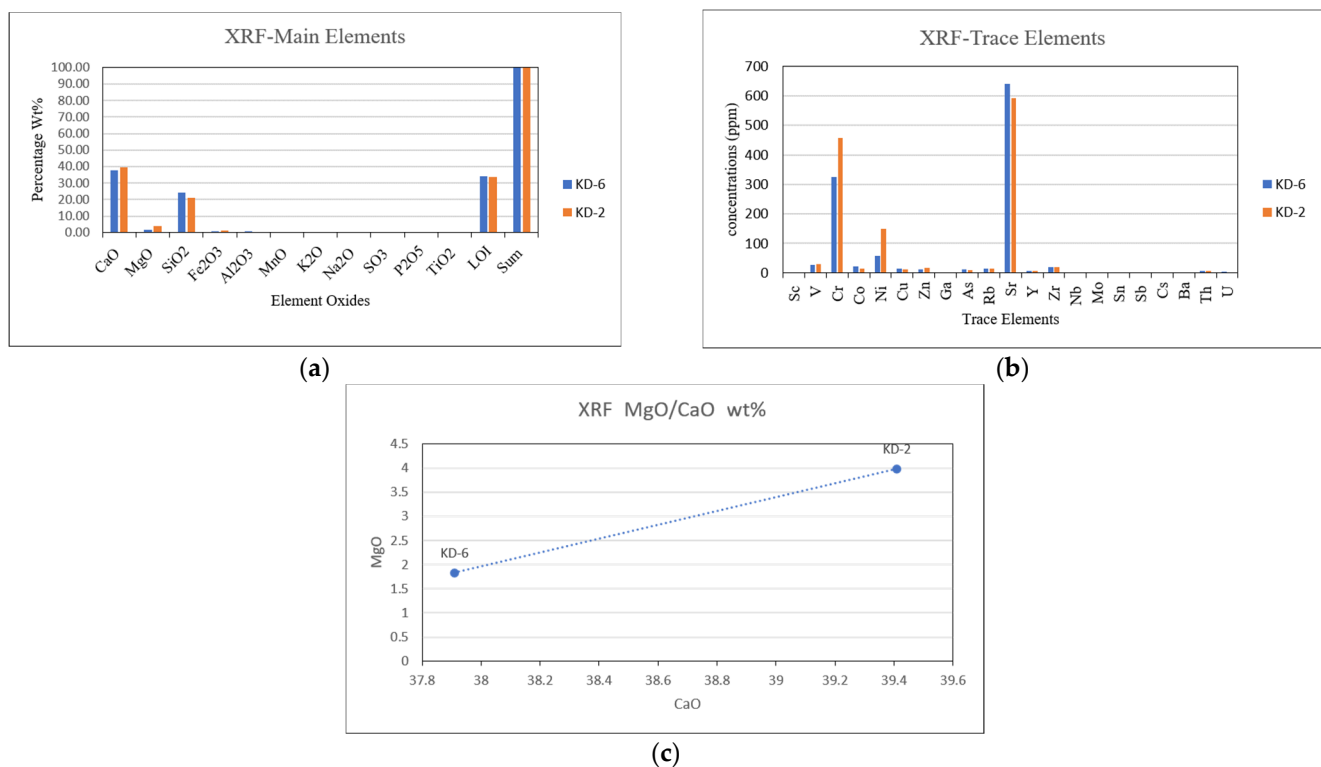
#### 4.1.4. Mineralogical and Chemical Analysis

Detailed X-ray diffraction analysis (XRD) of Diolkos samples (Figures S1–S7) showed that they are characterized by the presence of terrigenous minerals such as quartz, calcite, Mg-calcite, dolomite, plagioclase, K-feldspar and traces of serpentine and clay minerals

(illite, chlorite). Samples Kodi2 and Kodi3 are more abundant in Mg-calcite than the rest. The content in chlorite and serpentine is probably due to the presence of ultramafic sediments that are derived from ophiolites. Additionally, all Diolkos samples are abundant in calcite.

The results from the X-ray diffraction analysis of sample Sum2 from Sumuide showed the presence of carbonate minerals, such as Mg-calcite and aragonite.

The geochemistry of the beachrocks is in full accordance with the mineralogical/lithological characteristics of the samples. Table 3 presents the chemical composition of selected Diolkos samples, with the concentrations in major and trace elements of the samples analyzed using XRF. The mean concentration value of CaO of about 38.5% wt and the mean concentration of MgO of about 2.9% wt derive from both the sediment grains and the cement (Figure 5). The mean concentration of SiO<sub>2</sub> of about 22% wt derives only from the silicate sediment composition. The mean values of LOI (loss on ignition) reach a value of 33% wt. LOI's origination derives from the ignited carbonates. Thus, we count it as a part of both sediment and cement chemical imprint.



**Figure 5.** The abbreviations KD-2 and KD-6 stand for the XRF analysis of beachrock samples Kodi2 and Kodi6, respectively. (a) Bulk sample chemical analyses of major elements. All values are in wt. %. (b) Bulk sample chemical analyses of trace elements. All values are in ppm. (c) Comparison of MgO and CaO concentration values in wt. %.

Trace element concentrations (ppm) provided notable results concerning the presence of Cr and Ni, which show a higher concentration in the Kodi2 sample compared to Kodi6. The samples Kodi2 and Kodi6 showed Sr values of 591 ppm and 640 ppm, respectively. Strontium concentrations in water determine the sea water impact on the cementation process of beachrocks [53,54] and also reflect the weathering history of sediments [55].

## 4.2. Artificial Beachrocks Experiment Results

### 4.2.1. Microbial Population Count

In the case of Diolkos (experiment 1), we created a treatment solution of B1 bacteria, and their cell density was determined every day for a duration of 9 days. On day T0, the

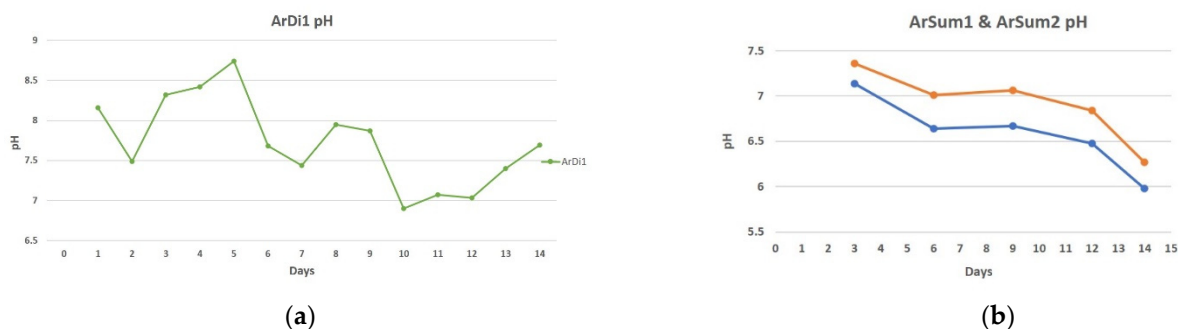
solution showed a 1400 nm ( $OD_{600}$ ) of B1, while it topped at 3790 nm ( $OD_{600}$ ) on day T3 and at 2200 nm on day T9 ( $OD_{600}$ ) (Figure 2).

In the case of Sumuide (experiments 2, 3), the density of bacteria B2 in the treatment solution was analyzed at time T: 0 h, 3 h, 6 h, 12 h, and 24 h (Figure 2). The high bacteria concentration treatment solution exceeds the limit of 2.200 nm ( $OD_{600}$ ) in the short time of 9 h. On the contrary, the low bacteria concentration treatment solution topped its measurement at 1.810 nm ( $OD_{600}$ ) in 24 h. We also used the bacteria of the high (experiment 2) and low concentration (experiment 3) solutions in order to create colonies while counting them. In experiment 2, bacteria cultivation had grown 62 colonies, while in experiment 3 bacteria cultivation had grown 19 colonies.

#### 4.2.2. pH and $Ca^{2+}$ Concentrations

The Diolkos artificial beachrock sample is hereafter called ArDi1 (experiment 1), the Sumuide sample with high bacteria concentration culture ( $OD_{600}/24\text{ h}$ : 2.2 nm) is ArSum1 (experiment 2) and the sample with low bacteria concentration culture ( $OD_{600}/24\text{ h}$ : 1.8 nm) is ArSum2 (experiment 3).

The solidification solution that we used for all experiments was maintained at pH 7.6–7.8. We applied/injected treatment solution daily for 14 days. In the case of the ArDi1 sample, the pH value showed a general rise trend until day 5 (with an exception on day 2, where there was a sharp drop). From day 5 until 7, the pH value had dropped to 7.5. On the same day (7), we reinjected bacterial culture solution, and on day 8 we noted a rise of the pH up to 7.9. However, the pH continued to drop until day 10, followed by a gentle rise until day 14, reaching up to 7.7 (Figure 6a).



**Figure 6.** pH values of (a) sample ArDi1 drain outlet, and (b) sample ArSum1, ArSum2 and no bacteria control sample drain outlet.

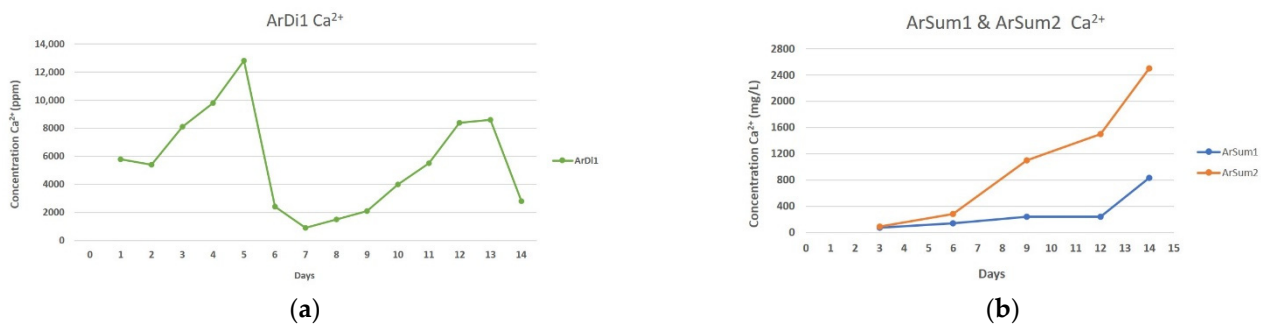
The pH value for both the ArSum1 and ArSum2 samples showed an increasing trend until day 3 of the experiment, and then decreased until day 6. On day 7, we reinjected bacterial culture solution in our experiment with the result of maintaining the pH until day 10. The dramatic change occurred on day 12, where a decreasing trend in the pH was observed (Figure 6b).

In all experiments, we added 20,000 ppm of  $Ca^{2+}$  daily. At time  $T = 0$  days, the experiment had the initial content of 20,000 ppm of  $Ca^{2+}$ . For sample ArDi1, the  $Ca^{2+}$  concentration in its drainage is characterized by a low concentration until day 2, followed by a rise until day 5. Day 7 is characterized by a dramatic fall of the  $Ca^{2+}$  concentration in the drainage, followed by a gentle rise until day 13 and concluding in day 14 with a decrease (Figure 7a).

The samples ArSum1 and ArSum2 are characterized by a constantly rising concentration of  $Ca^{2+}$  in their drainage (Figure 7b). On the third day of experiments, we measured almost the same values of  $Ca^{2+}$  in the outlet solution. A steady increase in concentration was observed until day 6. Even after the re-injection of bacterial culture solution on day 7, the ArSum2 sample tended to have an increase in the  $Ca^{2+}$  concentration in its drainage until the final day of the experiment. The sample ArSum1 showed a more stable trend in



$\text{Ca}^{2+}$  concentration in its drainage of 240 mg/L until the 12th day. On the final 2 days of the experiment, a rise in  $\text{Ca}^{2+}$  was observed in drainage.

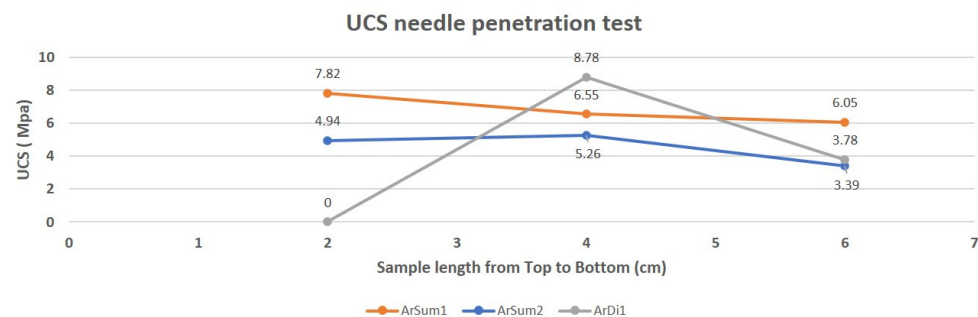


**Figure 7.**  $\text{Ca}^{2+}$  concentration in (a) sample ArDi1 drain outlet, (b) and in sample ArSum1 and ArSum2 drain outlet  $\text{Ca}^{2+}$  concentration.

#### 4.2.3. Solidification Test

The samples ArDi1, ArSum1 and ArSum2 were successfully solidified within the period of 14 days of treatment. The needle penetration test was applied on three parts of the sample (upper, middle, and bottom) in order to estimate the unconfined compressive strength (UCS). The Diolkos sample ArDi1 showed a decrease in UCS towards the bottom. The middle and the bottom showed mean values of 9 MPa and 3.6 MPa, respectively.

Subsequently, the samples ArSum1 and ArSum2 from Sumuide also showed a decrease in UCS from the upper to the bottom parts of the samples. The ArSum1 reached 7.82 MPa with a sample average value of 6.8 MPa. The ArSum2 reached 5.26 MPa with an average value of 4.53 MPa (Figure 8).



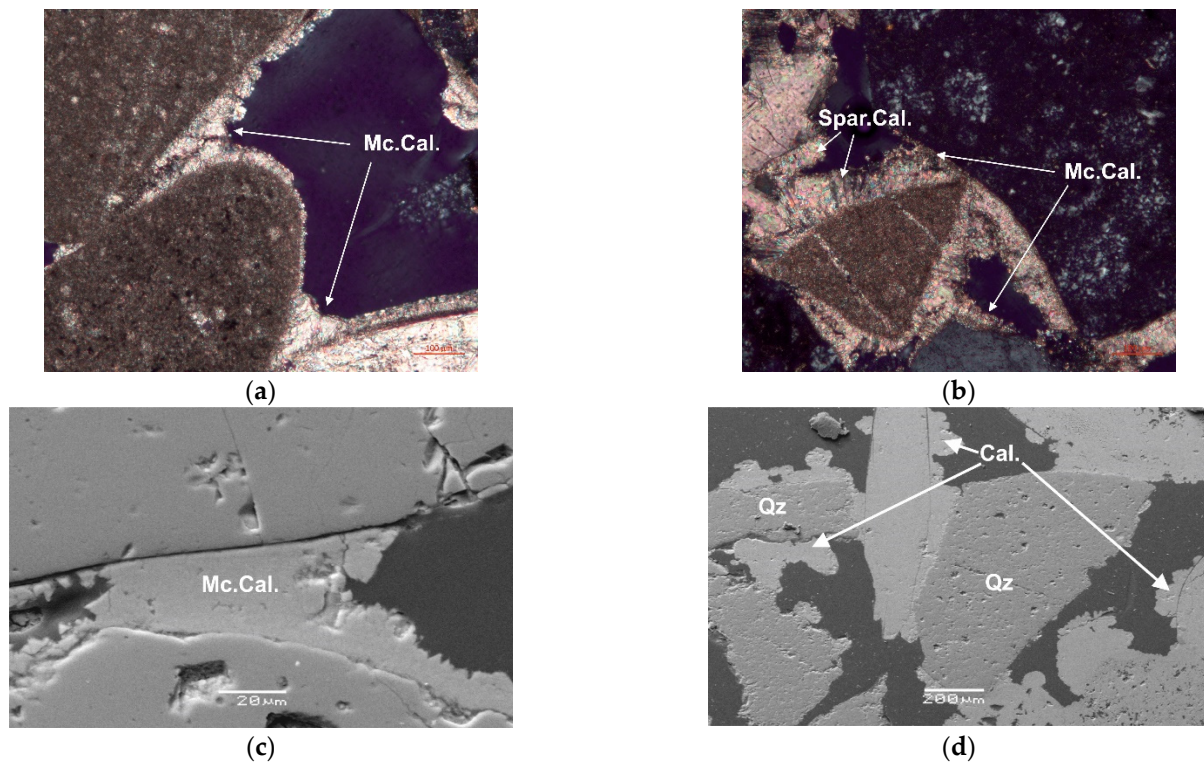
**Figure 8.** UCS estimated by needle penetration test of Diolkos artificial beachrock sample ArDi1 (grey line) and Okinawa artificial beachrock sample ArSum1 (orange line) and ArSum2 (blue line) in consideration of samples length from the top part (0 cm) to the bottom part (7 cm).

#### 4.2.4. Mineralogical Study and Geochemical Analysis of Artificial Beachrocks

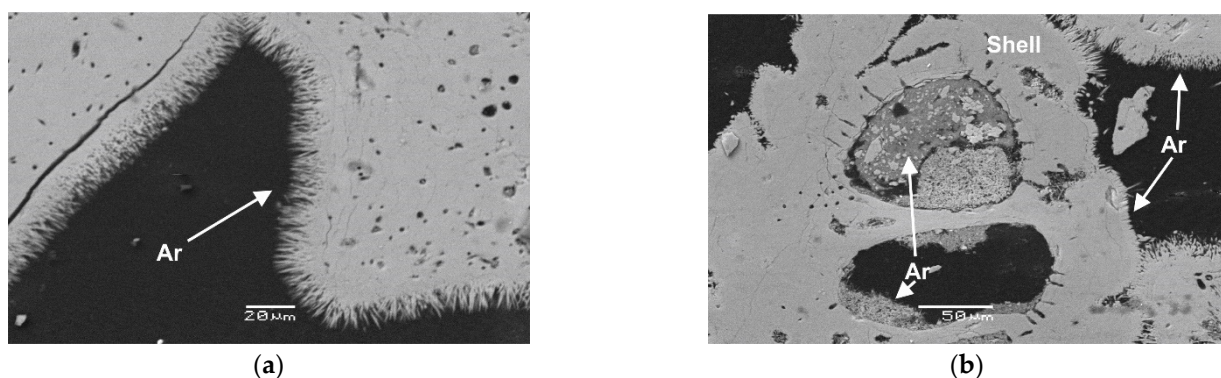
The artificial beachrocks were formed in vitro; thus, their physical characteristics were expected to be similar to the beach material. In the case of Diolkos sample (ArDi1), the lithoclasts are sub-rounded and poorly sorted, with a small contribution of bioclasts (<10%). The grains consisted of quartz, calcite, dolomite, albite and serpentine. The two artificial samples of Sumuide also showed a similar pattern to the corresponding natural beachrock: rounded and well-sorted grains with a high contribution of bioclasts (>60%), while the grains consisted of calcite, Mg-calcite and aragonite (Table 3).

The microscopic analysis of the three artificial beachrock samples showed that the sediment grains are similar in shape and composition with the natural beachrocks of the corresponding beaches. The cement of sample ArDi1, which was produced by the application of bacteria *Micrococcus yunnainensis* sp. and sand from the Diolkos area, is characterized by micritic and spirititic crystals of calcite in various sizes, from 10 µm to 100 µm. The crystal size and arrangement are regulated by the temperature, the calcium

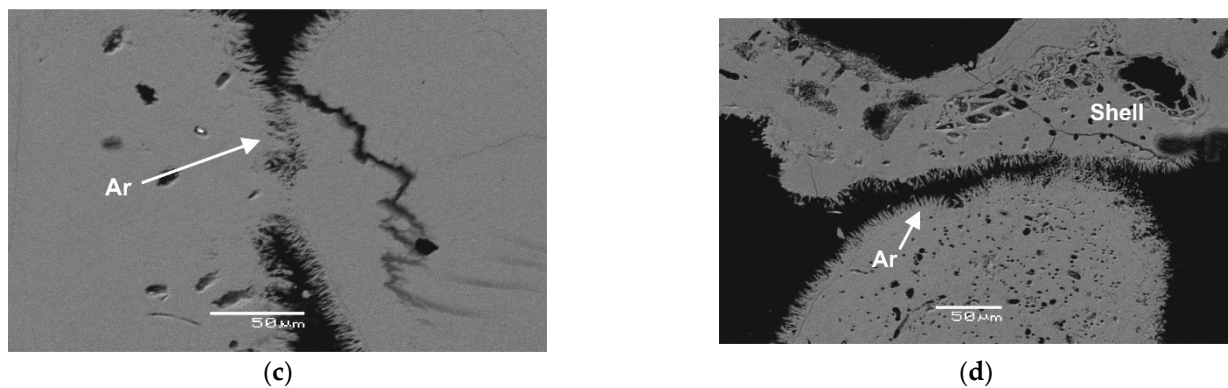
saturation and the gravitational forces. Additionally, a discontinuous fan shape grain coating was observed, along with microcrystalline calcite serving as pore filling with thick crystals of aragonite (Figure 9). The samples ArSum1 and ArSum2 were created by using coral sand and *Pararhodobacter* sp. bacteria of different concentrations from Sumuide. The two samples consisted of similar grain shape and composition to the local beachrock. Their cement was made of particularly well-developed aragonite crystals with lengths of around 10  $\mu\text{m}$  to 20  $\mu\text{m}$  (Figure 10).



**Figure 9.** Polarized microscopy image of sample ArDI1 at (a) 20x magnification, scale 100  $\mu\text{m}$ . Microcrystalline calcite cement is coating sediment grains and (b) 20x magnification, scale 100  $\mu\text{m}$ . Micritic and spirititic calcite cement forming fan shape grain coating. SEM images of sample ArDI1 (c) well developed calcite cement binding two sediment grains, (d) calcite cement forming the fan shape grain coating. Qz stands for quartz, Cal for calcite, Mc.Cal. for microcrystalline calcite and Spar. Cal. for spirititic calcite.



**Figure 10.** Cont.



**Figure 10.** SEM images of sample ArSum1 (a) well-developed crystals of aragonite cover the sediment grains and (b) crystals of aragonite and matrix cement work as pore filling in a foraminifera shell. SEM images of sample ArSum2 (c) well-developed crystals of aragonite binding two sediment grains, (d) general view of particles coated by aragonite crystals. Ar stands for aragonite.

## 5. Discussion

Beachrocks undoubtedly perform the role of a natural breakwater protecting the coast from erosion [31,56,57]. In this study, we identified the beachrock formation mechanism of Diolkos area, Corinth, Greece and Sumuide, Okinawa island, Japan. Additionally, analytical data were collected with the purpose of investigating the innovative method of MICP for creating artificial beachrocks as a proposal of a soft engineering countermeasure of sandy beach erosion.

Diolkos beachrock outcrop has a very compacted and thick morphology, which was also confirmed through optical and electron microscopy. The Diolkos beachrock outcrop has a mean thickness of 3 m, in contrast with the outcrop of Sumuide which was about 50 cm. In contrast with Diolkos' 10° inclination, Sumuide beachrock shows a very gentle inclination, almost parallel with the sea level. The sediment texture of the studied beachrocks is connected with the recent sedimentary processes of each area that supply material from the corresponding weathered bedrock. In Diolkos' case, there was a variety of consolidated lithoclasts, minerals and mineral grains with differences in their material density and hardness. The heterotropic erosion and sleeing of minerals has led to a variety of sizes in the consolidated sediment, from silt and very fine sand to pebbles and gravels. On the other hand, Sumuide beachrock sediment derives from the local coral reef of Okinawa Island and thus its texture is uniformly sandy with fossilized skeleton parts of foraminifera and coral parts.

### 5.1. Beachrock Cement

The cement of Diolkos beachrock is a typical high magnesium calcite (HMC) in micritic and sparitic crystal forms. Matrix cement was noted consisting of very fine sediment particles (silt) and micritic cement. The HMC micritic cement indicates marine provenance, but the matrix formation in the pores of the sediment indicates the mixing of sea and fresh water [18]. Combining the information of the cement type and cement texture, it is clear that Diolkos beachrock outcrop was formed by the combination of marine water and fresh water with a higher influence by the marine phase taking place in the upper intertidal zone.

The XRD analysis showed that the Diolkos beachrock is more abundant in Mg-calcite at its inner part (landward; samples Kodi2 and Kodi3) compared to its seaward part (samples Kodi4, Kodi5 and Kodi6). This difference in Mg-calcite was also noted by the XRF analysis and the correlation diagram of MgO/CaO (Figure 5c). Additionally, the XRF analysis showed that the inner part of Diolkos beachrock had high concentrations in Cr and Ni (Figure 5) that may have derived from the ophiolite outcrops, north of Loutraki city through torrents and small river estuaries.



Conversely, Sumuide beachrock is a different case. It is characterized by a well-developed coating of micritic HMC, with an abundance of sparitic calcite crystals and aragonite up to 20  $\mu\text{m}$  in size. The calcareous sediment composition favors the formation of calcite and coarse needle aragonite, which occasionally was recrystallized and formed smaller sparitic crystals. The coexistence of these different types of cement indicates a low intertidal/upper subtidal zone precipitation as it is mostly affected by the marine environment. These observations are in accordance with the XRD mineralogical analysis as the samples mainly consisted of Mg-calcite and aragonite. Additionally, it should be taken in account that tropical areas, such as Okinawa, have rainfalls with many millimeters of precipitation which can lead to a high water table level [58]. This leads to a mixed water (sea and fresh/meteoric water) cementation mechanism even if it occurs in the subtidal zone.

### 5.2. Artificial Beachrocks

The experiments for the artificial beachrocks were conducted taking into account two different considerations. During experiment 1 (sample ArDi1), the granulometry of the material used was similar to that of Diolkos beach. Conversely, during experiments 2 and 3, the granulometry of the samples was homogenous at 1 mm. The use of bacteria *Micrococcus yunnanensis* sp. (B1) and *Paradohobacter* sp. (B2) was defined due to their metabolic reaction that triggers the urease activity, which is followed by the  $\text{CaCO}_3$  precipitation; this is the main component of the MICP method.

During the solidification treatment of the artificial beachrock samples, pH and  $\text{Ca}^{2+}$  were measured from the outlet drainage. The reduction in pH during the treatment indicates the urease activity in the syringe samples (reaction 2). On the other hand,  $\text{Ca}^{2+}$  showed a reduced rate in the outlet drainage, which is due to the precipitation of  $\text{CaCO}_3$  (reaction 3) around the grains in the syringe. As the reaction proceeds, the calcium carbonate precipitates and forms aragonite and calcite cement.

The drainage of the ArDi1 sample showed high bacterial activity until the fifth day, the eighth day and during the last three days of experiment 1. The drainage of the ArSum1 sample showed higher values of pH and lower concentrations of  $\text{Ca}^{2+}$  than ArSum2. Both samples had the same pH trend, which showed a high bacterial activity until day 6. On day 7, a rise in the bacterial urease activity was noted until day 9. Although the second injection was applied, the pH did not rise to the initial value. These results suggest a difference in the samples' consolidation and physicochemical parameters.

Using the UCS needle penetration test on the middle and bottom part of ArDi1 samples, it was evident that the cementation was strong. The ArDi1 sample had a variety of sediment sizes, and this factor was important for the circulation of the solution in the pores. The upper part of ArDi1 had consolidated around a pebble that was 2 mm wide, along with sand particles of different sizes; thus, the UCS needle penetration test could not be applied on this part.

The UCS needle penetration test also confirmed that the Okinawa sample ArSum1 showed higher strength values than ArSum2; however, both samples were more compacted on their upper part than their lower (Figure 8). This could be due to the fact that the bottom resident bacteria were partially able to participate in the entire urease activity process. At the same time, the higher concentration of organic material at the bottom of the syringe due to bacteria mortality may also locally change the bacteria's living conditions. SEM images and EDS analysis have shown that the ArSum1 sample is characterized by coarse, well-developed crystals of aragonite cement in comparison to ArSum2, which did not have well-developed aragonite crystals, but had also additionally formed calcite cement.

Even though Sumuide artificial beachrocks consisted of 1 mm sand particles, which facilitated the solution circulation in the pores, the strength of the material was inferior to Diolkos artificial beachrock. Additionally, the particles' inhomogeneity in the ArDi1 sample and the resulting different porosity led to the precipitation of matrix cement, which also enhances the reduction in the pores. These findings reveal that the understanding of bacteria ureolysis ability plays a more important role than the particles' homogeneity.

All experimental conditions applied in this study showed the ability to create artificial beachrocks with specific physical and geochemical characteristics. The results of the artificial beachrock experiments highlight their potential to be used as an adaptation measure against coastal erosion. It has been noted by various authors [19,20,22,33,34] that sandy coasts hosting beachrocks are less affected by coastal erosion as beachrocks act as natural breakwaters that mitigate wave energy. Given the need for ecofriendly, sustainable and cost efficient coastal management measures, the MICP method to create artificial beachrocks [36,37,51,52,59] may play a crucial role in the future of soft engineering techniques.

## 6. Conclusions

Beachrocks are natural formations developed under specific physio-bio-chemical conditions. These formations are acting, in many cases, as breakwaters protecting the shore by the sea waves and their energy. Furthermore, they act as sediment traps if they are uplifted and stabilize the sandy beaches. In our case studies of (a) Diolkos, Greece and (b) Sumuide, Japan, we analyzed the beachrock formation mechanism by studying their natural characteristic and by simulating their formation using local bacteria and material. Diolkos beachrock was formed in the upper part of the intertidal zone, while it consisted of detrital material originating from the local bedrock. Sumuide beachrock was formed in the low intertidal–upper subtidal zone and it consisted of coral sand and foraminifera fragments. Their corresponding artificial samples showed similar physical and chemical results and properties. The results from the artificial beachrocks showed that the bacteria *Micrococcus yunnanensis* sp. of Diolkos created a more consolidated sample, with better physical characteristics than the bacteria *Pararhodobacter* sp. from the Sumuide area. The Sumuide artificial beachrocks showed that the bacterial density greatly affects the solidification result. Different parameters in the experiments have shown that the understanding of bacteria ureolysis ability plays a more important role than the particle homogeneity. Furthermore, the artificial beachrocks showed inferior but similar properties with their corresponding natural beachrocks.

Concluding, the artificial beachrock experiment may lead to a new era of a sustainable soft engineering constructions where we can imitate the natural beachrock characteristic as a break water. By creating artificial beachrocks in vulnerable sandy beaches affected by erosion, we achieve ecofriendly coastal sustainability while (a) saving energy as this method does not need large amounts of any type of energy, (b) reducing CO<sub>2</sub> emissions as this method does not involve cement, and (c) building materials due to the fact of using the local beach material. Finally, artificial beachrocks, by sharing the same natural principles as the natural occurrences, may have a positive impact on marine biodiversity as they will play the role of rocky habitats for fisheries, algae, microorganisms, etc.

**Supplementary Materials:** The following are available online at <https://www.mdpi.com/article/10.3390/jmse10010087/s1>, Figure S1: XRD analyses of beachrock sample from natural Okinawa beachrock, sample Sum2. Figure S2: XRD analyses of artificial beachrock sample from Okinawa beachrock ArSum1. Figure S3: XRD analyses of beachrock sample from natural Diolkos beachrock Kodi2. Figure S4: XRD analyses of beachrock sample from natural Diolkos beachrock Kodi3. Figure S5: XRD analyses of beachrock sample from natural Diolkos beachrock Kodi4. Figure S6: XRD analyses of beachrock sample from natural Diolkos beachrock Kodi5. Figure S7: XRD analyses of beachrock sample from natural Diolkos beachrock Kodi6.

**Author Contributions:** Conceptualization, G.S.; methodology, G.S., N.E., S.K., E.K. and A.K.; investigation, G.S. and E.K.; writing—original draft preparation, G.S., A.K. and E.K.; writing—review and editing, G.S., A.K., E.K., K.T., S.K. and N.E.; visualization, G.S.; supervision, N.E. and S.K. All authors have read and agreed to the published version of the manuscript.

**Funding:** This research received no external funding.

**Institutional Review Board Statement:** Not applicable.



**Informed Consent Statement:** Not applicable.

**Data Availability Statement:** Not applicable.

**Acknowledgments:** The present work was co-funded by the European Union and Greek national funds through the Operational Program “Human Resources Development, Education and Lifelong Learning” (NSRF 2014–2020), under the call “Supporting Researchers with an Emphasis on Young Researchers—Cycle B” (MIS: 5047955).

**Conflicts of Interest:** The authors declare no conflict of interest.

## References

- Luijendijk, A.; Hagenaars, G.; Ranasinghe, R.; Baart, F.; Donchyts, G.; Aarninkhof, S. The State of the World’s Beaches. *Sci. Rep.* **2018**, *8*, 6641. [CrossRef] [PubMed]
- Floriani, D.C.; Fukuda, J.C.; Pinto, E.F. Lençóis Maranhenses National Park: The largest coastal dunes area in South America. *Gerenc. Costeiro Integr.* **2004**, *2*, 62–64.
- Barbier, E.B.; Georgiou, I.Y.; Enchelmeier, B.; Reed, D.J. The Value of Wetlands in Protecting Southeast Louisiana from Hurricane Storm Surges. *PLoS ONE* **2013**, *8*, e58715. [CrossRef]
- World Tourism Organisation. *UNWTO Tourism Highlights*, 2001st ed.; The World Tourism Organization: Madrid, Spain, 2001.
- Vousdoukas, M.I.; Ranasinghe, R.; Mentaschi, L.; Plomaritis, T.A.; Athanasiou, P.; Luijendijk, A.; Feyen, L. Sandy coastlines under threat of erosion. *Nat. Clim. Chang.* **2020**, *10*, 260–263. [CrossRef]
- Van der Weide, J.; de Vroeg, H.; Sanyang, F. Guidelines for coastal erosion management. In Proceedings of the Fifth International Conference on the Mediterranean Coastal Environment: MEDCOAST 01, Hammamet, Tunisia, 23–27 October 2001; MEDCOAST: Ankara, Turkey, 2001; Volume 3, pp. 1399–1414.
- Gillie, R.D. Special Issue No. 24. Island States at Risk: Global Climate Change. *J. Coast. Res.* **1997**, 173–204. Available online: <https://af.booksc.eu/book/28517257/8b083c> (accessed on 5 January 2022).
- Weerakkody, U. Potential Impact of Accelerated Sea-Level Rise on Beaches of Sri Lanka. *J. Coast. Res.* **1997**, 225–242. Available online: <https://www.jstor.org/stable/25736096> (accessed on 5 January 2022).
- Basco, D.R. Misconceptions about seawall and beach interactions. In Proceedings of the Land-ocean interactions: Managing Coastal Ecosystems, Antalya, Turkey, 9–13 November 1999; Volume 3, pp. 1565–1578. Available online: [https://books.google.com.hk/books/about/Land\\_ocean\\_interactions\\_managing\\_coastal.html?id=0ASazgEACAAJ&redir\\_esc=y](https://books.google.com.hk/books/about/Land_ocean_interactions_managing_coastal.html?id=0ASazgEACAAJ&redir_esc=y) (accessed on 5 January 2022).
- Wiegel, R.L. Seawalls, Seacliffs, Beachrock: What Beach Effects? Part 1. In Proceedings of the Shore and Beach, 2002; Volume 1, p. 70, pp. 17–27. Available online: <https://www.google.com.hk/url?sa=t&source=web&cd=&cad=rja&uact=8&ved=2ahUKewi8psjhuZ71AhWmmGoFHRzwbQ8QFnoECAQQAQ&url=https%3A%2F%2Fwww.researchgate.net%2Fpublication/26publicationUId%3D313048443&usg=AOvVaw2OxI9SobEKSbtIvPVwopOO> (accessed on 5 January 2022).
- Phillips, M.R.; Jones, A.L. Erosion and tourism infrastructure in the coastal zone: Problems, consequences and management. *Tour. Manag.* **2006**, *27*, 517–524. [CrossRef]
- Cooper, J.A.G.; Mckenna, J. Working with natural processes: The challenge for coastal protection strategies. *Geogr. J.* **2008**, *174*, 315–331. [CrossRef]
- Schoonees, T.; Gijón Mancheño, A.; Scheres, B.; Bouma, T.J.; Silva, R.; Schlurmann, T.; Schüttrumpf, H. Hard Structures for Coastal Protection, Towards Greener Designs. *Estuaries Coasts* **2019**, *42*, 1709–1729. [CrossRef]
- IPCC. *Climate Change 2013—The Physical Science Basis*; Intergovernmental Panel on Climate Change, Ed.; Cambridge University Press: Cambridge, UK, 2014; ISBN 9781107415324.
- Brown, S.; Nicholls, R.J.; Hanson, S.; Brundrit, G.; Dearing, J.A.; Dickson, M.E.; Gallop, S.L.; Gao, S.; Haigh, I.D.; Hinkel, J.; et al. Shifting perspectives on coastal impacts and adaptation. *Nat. Clim. Chang.* **2014**, *4*, 752–755. [CrossRef]
- IPCC. Summary for Policymakers. In *IPCC Special Report on the Ocean and Cryosphere in a Changing Climate*; Pörtner, H.-O., Roberts, D.C., Masson-Delmotte, V., Zhai, P., Tignor, M., Poloczanska, E., Mintenbeck, K., Alegría, A., Nicolai, M., Okem, A., et al., Eds.; IPCC: Geneva, Switzerland, 2019.
- Vousdoukas, M.I.; Velegrakis, A.F.; Plomaritis, T.A. Beachrock occurrence, characteristics, formation mechanisms and impacts. *Earth-Sci. Rev.* **2007**, *85*, 23–46. [CrossRef]
- Mauz, B.; Vacchi, M.; Green, A.; Hoffmann, G.; Cooper, A. Beachrock: A tool for reconstructing relative sea level in the far-field. *Mar. Geol.* **2015**, *362*, 1–16. [CrossRef]
- Karkani, A.; Evelpidou, N.; Vacchi, M.; Morhange, C.; Tsukamoto, S.; Frechen, M.; Maroukian, H. Tracking shoreline evolution in central Cyclades (Greece) using beachrocks. *Mar. Geol.* **2017**, *388*, 25–37. [CrossRef]
- Evelpidou, N.; Kawasaki, S.; Karkani, A.; Saitis, G.; Spada, G.; Economou, G. Evolution of relative sea level in Okinawa (Japan) during Holocene. *Geogr. Fis. Din. Quat.* **2019**, *42*, 3–16.
- Polidorou, M.; Saitis, G.; Evelpidou, N. Beachrock development as an indicator of paleogeographic evolution, the case of Akrotiri Peninsula, Cyprus. *Z. Geomorphol.* **2021**, *63*, 3–17. [CrossRef]

22. Saitis, G.; Koutsopoulou, E.; Karkani, A.; Anastasatou, M.; Stamatakis, M.; Gatou, M.A.; Evelpidou, N. A multi-analytical study of beachrock formation in Naxos and Paros Islands, Aegean Sea, Greece and their palaeoenvironmental significance. *Z. Geomorphol.* **2021**, *63*, 19–32. [\[CrossRef\]](#)
23. Bricker, O.P. Introduction: Beachrock and intertidal cement. In *Carbonate Cements*; Bricker, O.P., Ed.; Johns Hopkins Press: Baltimore, MD, USA, 1971; pp. 1–13.
24. Tucker, M.E.; Wright, V.P. *Carbonate Sedimentology*; Blackwell Science Ltd.: Oxford, UK, 1990; ISBN 0632014725.
25. Alexandersson, T. Intragranular Growth of Marine Aragonite and Mg-Calcite: Evidence of Precipitation from Supersaturated Seawater. *J. Sediment. Res.* **1972**, *42*, 441–460. [\[CrossRef\]](#)
26. Scholle, P.A.; Bebout, D.G.; Moore, C.H. *Carbonate Depositional Environments*; Scholle, P.A., Bebout, D.G., Moore, C.H., Eds.; The American Association of Petroleum Geologists: Tulsa, OK, USA, 1983; ISBN 0891813101.
27. Mauz, B.; Ruggieri, G.; Spada, G. Terminal Antarctic melting inferred from a far-field coastal site. *Quat. Sci. Rev.* **2015**, *116*, 122–132. [\[CrossRef\]](#)
28. Hanor, J.S. Precipitation of beachrock cements: Mixing of marine and meteoric waters vs. CO<sub>2</sub>-degassing. *J. Sediment. Res.* **1978**, *48*, 498–501.
29. Molenaar, N.; Venmans, A.A.M. Calcium carbonate cementation of sand: A method for producing artificially cemented samples for geotechnical testing and a comparison with natural cementation processes. *Eng. Geol.* **1993**, *35*, 103–122. [\[CrossRef\]](#)
30. Bernier, P.; Guidi, J.-B.; Böttcher, M.E. Coastal progradation and very early diagenesis of ultramafic sands as a result of rubble discharge from asbestos excavations (northern Corsica, western Mediterranean). *Mar. Geol.* **1997**, *144*, 163–175. [\[CrossRef\]](#)
31. Danjo, T.; Kawasaki, S. Characteristics of Beachrocks: A Review. *Geotech. Geol. Eng.* **2014**, *32*, 215–246. [\[CrossRef\]](#)
32. Khan, M.N.H.; Shimazaki, S.; Kawasaki, S. Coral sand solidification test through microbial calcium carbonate precipitation using *Pararhodobacter* sp. *Int. J. Geomate* **2016**, *11*, 2665–2670. [\[CrossRef\]](#)
33. Voudoukas, M.I.; Velegrakis, A.F.; Karambas, T.V. Morphology and sedimentology of a microtidal beach with beachrocks: Vatera, Lesbos, NE Mediterranean. *Cont. Shelf Res.* **2009**, *29*, 1937–1947. [\[CrossRef\]](#)
34. Psomiadis, D.; Albanakis, K.; Tsourlos, P. Evaluation of Sea-Level Rise Impact on Cemented and Uncemented Beach. Case Study From Thassos Island. In Proceedings of the Scientific Annals, XIX CBGA Congress, Thessaloniki, Greece, 23–26 September 2010; Volume 99, pp. 483–490.
35. Khan, M.N.H.; Danjo, T.; Kawasaki, S. Artificial beachrock formation through sand solidification towards the inhibit of coastal erosion in Bangladesh. *Int. J. Geomate* **2015**, *9*, 1528–1533. [\[CrossRef\]](#)
36. Fujita, M.; Nakashima, K.; Achal, V.; Kawasaki, S. Whole-cell evaluation of urease activity of *Pararhodobacter* sp. isolated from peripheral beachrock. *Biochem. Eng. J.* **2017**, *124*, 1–5. [\[CrossRef\]](#)
37. Khan, M.N.H.; Kawasaki, S. Making Artificial Beachrock Through Bio-cementation: A Novel Technology to Inhibition of Coastal Erosion. In *Handbook of Environmental Materials Management*; Hussain, C.M., Ed.; Springer International Publishing: Cham, Switzerland, 2018; pp. 1–24. ISBN 978-3-319-58538-3.
38. Daryono, L.R.; Titisari, A.D.; Warmada, I.W.; Kawasaki, S. Comparative characteristics of cement materials in natural and artificial beachrocks using a petrographic method. *Bull. Eng. Geol. Environ.* **2019**, *78*, 3943–3958. [\[CrossRef\]](#)
39. Whiffin, V.S.; van Paassen, L.A.; Harkes, M.P. Microbial carbonate precipitation as a soil improvement technique. *Geomicrobiol. J.* **2007**, *24*, 417–423. [\[CrossRef\]](#)
40. Rahman, M.M.; Hora, R.N.; Ahenkorah, I.; Beecham, S.; Karim, M.R.; Iqbal, A. State-of-the-art review of microbial-induced calcite precipitation and its sustainability in engineering applications. *Sustainability* **2020**, *12*, 6281. [\[CrossRef\]](#)
41. Al Imran, M.; Kimura, S.; Nakashima, K.; Evelpidou, N.; Kawasaki, S. Feasibility study of native ureolytic bacteria for biocementation towards coastal erosion protection by MICP method. *Appl. Sci.* **2019**, *9*, 4462. [\[CrossRef\]](#)
42. Higgins, M.D.; Higgins, R.A. A geological companion to Greece and the Aegean. *Choice Rev. Online* **1993**, 34–3874. [\[CrossRef\]](#)
43. Maroukian, H.; Gaki-Papanastassiou, K.; Papanastassiou, D. Coastal changes in Corinthia, Greece. In Proceedings of the Maritimae: Cyprus and the Eastern Mediterranean from Prehistory to Late Antiquity, Nicosia, Cyprus, 18–22 October 1994; Scholars Press: Atlanta, GA, USA, 1994; pp. 217–225; Available online: [https://www.google.com.hk/url?sa=t&rct=j&q=&esrc=s&source=web&cd=&cad=rja&uact=8&ved=2ahUKEwjNue2zu571AhWSIWofHSMJCIMQFnoECAQQAQ&url=http%3A%2F%2Fwww.worldcat.org%2Ftitle%2Fres-maritimae-cyprus-and-the-eastern-mediterranean-from-prehistory-to-late-antiquity-proceedings-of-the-second-international-symposium-cities-on-the-sea-nicosia-cyprus-october-18-22-1994%2Foclc%2F37725534%26referer%3Dbrief\\_results&usq=AOvVaw0G4CXo0IRUizuoWrsyYkKr](https://www.google.com.hk/url?sa=t&rct=j&q=&esrc=s&source=web&cd=&cad=rja&uact=8&ved=2ahUKEwjNue2zu571AhWSIWofHSMJCIMQFnoECAQQAQ&url=http%3A%2F%2Fwww.worldcat.org%2Ftitle%2Fres-maritimae-cyprus-and-the-eastern-mediterranean-from-prehistory-to-late-antiquity-proceedings-of-the-second-international-symposium-cities-on-the-sea-nicosia-cyprus-october-18-22-1994%2Foclc%2F37725534%26referer%3Dbrief_results&usq=AOvVaw0G4CXo0IRUizuoWrsyYkKr) (accessed on 5 January 2022).
44. Gungor, A.; Lee, G.H.; Kim, H.J.; Han, H.C.; Kang, M.H.; Kim, J.; Sunwoo, D. Structural characteristics of the northern Okinawa Trough and adjacent areas from regional seismic reflection data: Geologic and tectonic implications. *Tectonophysics* **2012**, *522*–523, 198–207. [\[CrossRef\]](#)
45. Wang, Z.; Hu, P.; Gaetani, G.; Liu, C.; Saenger, C.; Cohen, A.; Hart, S. Experimental calibration of Mg isotope fractionation between aragonite and seawater. *Geochim. Cosmochim. Acta* **2013**, *102*, 113–123. [\[CrossRef\]](#)
46. Danjo, T.; Kawasaki, S. Formation mechanisms of beachrocks in okinawa and Ishikawa, Japan, with a focus on cements. *Mater. Trans.* **2014**, *55*, 493–500. [\[CrossRef\]](#)
47. Danjo, T.; Kawasaki, S. A study of the formation mechanism of beachrock in Okinawa, Japan: Toward making artificial rock. *Int. J. Geomate* **2013**, *5*, 634–639. [\[CrossRef\]](#)

48. Desruelles, S.; Fouache, É.; Ciner, A.; Dalongeville, R.; Pavlopoulos, K.; Kosun, E.; Coquinot, Y.; Potdevin, J.L. Beachrocks and sea level changes since Middle Holocene: Comparison between the insular group of Mykonos-Delos-Rhenia (Cyclades, Greece) and the southern coast of Turkey. *Glob. Planet. Change* **2009**, *66*, 19–33. [\[CrossRef\]](#)
49. Vacchi, M.; Rovere, A.; Zouros, N.; Desruelles, S.; Caron, V.; Firpo, M. Spatial distribution of sea-level markers on Lesbos Island (NE Aegean Sea): Evidence of differential relative sea-level changes and the neotectonic implications. *Geomorphology* **2012**, *159–160*, 50–62. [\[CrossRef\]](#)
50. Petropoulos, A.; Baziotis, I.; Anagnostou, C.; Evelpidou, N. Beachrocks Cement Characteristics and Conditions of Formation. Case Study Platani Beach, Chania, Greece. *Bull. Geol. Soc. Greece* **2017**, *50*, 458. [\[CrossRef\]](#)
51. Al Imran, M.; Nakashima, K.; Evelpidou, N.; Kawasaki, S. Factors affecting the urease activity of native ureolytic bacteria isolated from coastal areas. *Geomech. Eng.* **2019**, *17*, 421–427. [\[CrossRef\]](#)
52. Danjo, T.; Kawasaki, S. Microbially induced sand cementation method using *pararhodobacter* sp. strain SO1, inspired by beachrock formation mechanism. *Mater. Trans.* **2016**, *57*, 428–437. [\[CrossRef\]](#)
53. Guerra, N.C.; Kiang, C.H.; Sial, A.N. Carbonate cements in contemporaneous beachrocks, Jaguaribe beach, Itamaracá island, northeastern Brazil: Petrographic, geochemical and isotopic aspects. *An. Acad. Bras. Ciências* **2005**, *77*, 343–352. [\[CrossRef\]](#)
54. Sunagawa, I.; Takahashi, Y.; Imai, H. Strontium and aragonite-calcite precipitation. *J. Mineral. Petrol. Sci.* **2007**, *102*, 174–181. [\[CrossRef\]](#)
55. McLennan, S.M.; Hemming, S.; McDaniell, D.K.; Hanson, G.N. Geochemical approaches to sedimentation, provenance, and tectonics. In *Processes Controlling the Composition of Clastic Sediments*; Geological Society of America: Boulder, CO, USA, 1993; p. 21.
56. Voudoukas, M.; Velegrakis, A.F.; Karambas, T.; Valais, G.; Zarkogiannis, S. Morphodynamics of beachrock infected beaches: Vatera Beach, Northeastern Mediterranean. In Proceedings of the Fifth International Conference on Coastal Dynamics, Barcelona, Spain, 4–8 April 2005. [\[CrossRef\]](#)
57. Daryono, L.R.; Nakashima, K.; Kawasaki, S.; Titisari, A.D.; Barianto, D.H. Sediment Characteristics of Beachrock: A Baseline Investigation Based on Microbial Induced Carbonate Precipitation at Krakal-Sadranan Beach, Yogyakarta, Indonesia. *Appl. Sci.* **2020**, *10*, 520. [\[CrossRef\]](#)
58. Ikema, T.; Bigg, G.R.; Bryant, R.G. Increasing rain intensity over Okinawa, 1982–2005, and the link to changes in characteristics of northwest Pacific typhoons. *J. Geophys. Res. Atmos.* **2010**, *115*, 24121. [\[CrossRef\]](#)
59. Daryono, L.R.; Nakashima, K.; Kawasaki, S.; Suzuki, K. Investigation of Natural Beachrock and Physical—Mechanical Comparison with Artificial Beachrock Induced by MICP as a Protective Measure against Beach Erosion at Yogyakarta, Indonesia. *Geosciences* **2020**, *10*, 143. [\[CrossRef\]](#)